Energy Flow and Functional Behavior of Individual Muscles at Different Speeds During Human Walking

Zheqi Hu, Lei Ren, *Member, IEEE*, Guowu Wei, *Member, IEEE*, Zhihui Qian, Wei Liang, Wei Chen, Xuewei Lu, Luquan Ren, and Kunyang Wang, *Member, IEEE*

***Abstract*— Understanding the distinct functions of human muscles could not only help professionals obtain insights into the underlying mechanisms that we accommodate compromised neuromuscular system, but also assist engineers in developing rehabilitation devices. This study aims to determine the contribution of major muscle and the energy flow in the human musculoskeletal system at four sub-phases (collision, rebound, preload, push-off) during the stance of walking at different speeds. Gait experiments were performed with three self-selected speeds: slow, normal, and fast. Muscle forces and mechanical work were calculated by using a subject-specified musculoskeletal model. The functions of individual muscles were characterized as four functional behaviors (strut, spring, motor, damper), which were determined based on the mechanical energy. The results showed that during collision, hip flexors (iliacus and psoas major) and ankle dorsiflexors (anterior tibialis) were the most dominant muscles in buffering the stride with energy absorption; during rebound, the posterior muscles (gluteus maximus, gastrocnemius, posterior tibialis, soleus) contributed the most to energy generation; during preload, energy for preparing push-off was mainly absorbed by the muscles surrounding knee (vastus, semimembranosus, semitendinosus); during push-off, ankle plantar flexors (gastrocnemius, soleus, posterior tibialis, peroneus muscles, flexor digitorum, flexor hallucis) mainly behaved to generate energy for forward propulsion. With increased walking speed, additional energy (almost 400%) from harder stride was mainly absorbed by the flexor muscles. Hip extensors and adductors transferred more energy (around 150%) to the distal segments during rebound. Soleus and gastrocnemius muscles generated more energy (about 75%) to the proximal segments for propulsion. Along with our previous study of joint-level energy analysis, these findings could assist better understanding of human musculoskeletal behaviors during locomotion and provide principles for the bio-design of related assistive devices from motors performance enhancement to rehabilitation such as exoskeleton and prosthesis.**

***Index Terms*— Rehabilitation, muscle function, energy flow, biomechanics, walking speed, musculoskeletal model.**

Manuscript received 3 February 2022; revised 23 October 2022; accepted 9 November 2022. Date of publication 14 November 2022; date of current version 31 January 2023. This work was supported in part by the National Key Research and Development Program of China under Grant 2018YFC2001300; in part by the National Natural Science Foundation of China under Grant 52005209, Grant 91948302, Grant 91848204, and Grant 52021003; and in part by the Natural Science Foundation of Jilin Province under Grant 20210101053JC. *(Corresponding authors: Lei Ren; Kunyang Wang.)*

Zheqi Hu and Lei Ren are with the Key Laboratory of Bionic Engineering, Ministry of Education, Jilin University, Changchun 130025, China, and also with the School of Mechanical, Aerospace and Civil Engineering, University of Manchester, M13 9PL Manchester, U.K. (e-mail: lren@jlu.edu.cn).

Guowu Wei is with the School of Science, Engineering and Environment, University of Salford, M5 4WT Salford, U.K.

Zhihui Qian, Luquan Ren, and Kunyang Wang are with the Key Laboratory of Bionic Engineering, Ministry of Education, Jilin University, Changchun 130025, China, and also with the Weihai Institute for Bionics, Jilin University, Weihai 264402, China (e-mail: kywang@jlu.edu.cn).

Wei Liang and Wei Chen are with the Key Laboratory of Bionic Engineering, Ministry of Education, Jilin University, Changchun 130025, China.

Xuewei Lu is with the School of Mechanical, Aerospace and Civil Engineering, University of Manchester, M13 9PL Manchester, U.K.

This article has supplementary downloadable material available at https://doi.org/10.1109/TNSRE.2022.3221986, provided by the authors.

Digital Object Identifier 10.1109/TNSRE.2022.3221986

I. Introduction

WALKING is one of the most significant activities in human daily living. Human walking is the result of energy generation and absorption [1], which is performed by muscle contractions and soft tissue deformations. The mechanical energy performance is often analyzed at joint and segment level [2], [3], [4], [5]. However, muscles produce mechanical work to support and propel the body moving as the energy sources [6]. Learning the operating functions of these muscles would be important not only for understanding the biomechanical constraints on locomotor ability, but also for obtaining insights into the underlying mechanisms that determine the way we move and adapt to accommodate compromised neuromuscular system function. In turn, this information would provide fundamental principles for the bio-inspired design of assistive devices related to human locomotion, from motors performance enhancement to rehabilitation (e.g., exoskeletons, prostheses, or rehabilitation robots).

Muscles perform a range of functions with different tasks [7], [8]. Their functions can be characterized into four different behaviors based on mechanical work performance: strut-like to generate great force with minimal length altering; spring-like to store and return elastic strain energy; motor-like to generate positive mechanical energy; damper-like to absorb

mechanical energy [6], [9]. The functions of muscles can be affected by anatomical location and task demands [10], [11], [12]. For example, Neptune et al. [10] analyzed redistribution of segmental powers by muscle forces during human walking and quantified the contributions of individual muscles to body progression. Distal muscles mainly contribute as strut [13], and proximal muscles mainly contribute to work modulation [14] during locomotion. Another study showed that human ankle plantar flexor work changed with a shift in whole body mechanical demands during sprinting [15]. These studies mainly focus on studying muscle function during a whole gait cycle or whole stance phase. However, the stance phase can be divided into four sub-phases: collision, rebound, preload and push-off based on work rate of the center of mass (COM) [16]. It is unclear what functional behaviors of individual muscles are and whether they will change during different sub-phases.

Humans can walk over a wide range of speeds with remarkable efficiency. Knowing the muscle energy flow and function change with different speeds would be important for better understanding how the muscles modulate the amount of mechanical power that the lower limbs absorb and output during walking. Hof et al. [17] showed that the average electromyography (EMG) profiles had considerable differences with speeds. Ivanenko et al. [18] presented that the different muscles were activated at different stepping speeds and the activity patterns were basically the same across speeds. As for one specific muscle, the behavior shifts with locomotion speed and gait. Farris and Sawicki [11] found that the fascicle-shortening velocity of human medial gastrocnemius at the time of peak muscle force production increased with walking speed, impairing the ability of the muscle to produce high peak forces. These studies, however, have not been attempted to systematically quantify the energy flow changes between the major muscle groups under varied walking speeds.

In this study, we investigated the muscle-level mechanical work and distinct functional behaviors interaction in each of the four sub-phases (collision, rebound, preload and push-off) during the stance of walking at different speeds (slow, normal, and fast). By combining the energy flow with muscle function, a muscle's contribution to a specific movement or event can be quantified. This approach could resolve many conflicting interpretations of muscle function that were based on correlation between EMG data and the ongoing gait mechanics. A 3D motion capture system integrated with a force plate array was used to measure the kinematic and kinetic data. The mechanical power and work of the individual muscles were calculated from inverse dynamic analysis by using a subject-specified musculoskeletal model. The functional behaviors of the muscle were determined based on the mechanical energy produced by muscles, defined as the sum of the mechanical work at origin and insertion point. The directions and magnitudes of muscle energy flow during four sub-phases were then obtained. Based on the conclusion from joint level analysis [4], we hypothesized that the muscles surrounding hip and ankle were the main contributors to walking during collision and push-off. This study would advance the understanding of muscle-level energy transmission and functional interactions in the human body during walking at different speeds, which could benefit rehabilitation and bionic designs of assistive devices such as exoskeleton and prosthesis.

II. Materials and Methods

A. Gait Measurement

Ten healthy adults with no previous medical history of bone or joint injury ($N = 10$, all males; weight 84.0±15.1 kg; height 1.76±0.07 m; mean±s.d.) participated in this study. These subjects were previously provided written informed consent before participation and separately provided written consent in accordance with the policies of the ethical committee of the university. They were asked to walk on the walkway under three different self-selected speeds: fast (1.82±0.36 m/s), normal (1.51±0.32 m/s), and slow (1.25±0.27 m/s). Each walking speed was measured 10 times. Kinematic data was collected at 200 Hz using a six-infrared camera motion capture system (Vicon, UK), and ground reaction force/moment data were recorded at 1000 Hz by using a three-force plate array (Kistler, Switzerland).

A group of specially designed thermoplastic plates [19] were attached to the 13 body segments, each with a cluster of four reflective markers. The head marker cluster was hold by a helmet. The plastic plate holding the pelvis marker cluster has been firmly fixed by an elastic hip belt. Plastic plates and the helmet reduce the relative movement between the markers on a segment, thereby improving the accuracy of the measured data [20], [21].

The anatomical landmarks were located from a series of static calibration procedures by using a calibration wand and reflective markers. The calibration markers were then removed before walking tests according to the calibrated anatomical system technique [22]. The functional approach [23], [24] was used to determine the hip joint center. Other joint centers were defined based on anatomical landmarks.

B. Calculation of Individual Muscle Energy Flow

With after-processed data, muscle forces were determined in an open source software OpenSim [25]. A subject-specified musculoskeletal model was built, including scaled segment models and muscle models. The scaling parameters were determined based on the static measurement data. Each individual muscle was modelled as a Hill-type unit with contractile and series elastic elements [26]. With the results of joint kinematics and kinetics, muscles forces were computed from the Residual Reduction Algorithm (RRA) and Computed Muscle Control (CMC) tool. Computed muscle control (CMC) was used to evaluate the muscle forces based on the measured motion data and ground reactions from the gait measurements [27]. Then, the muscle power P_{muscle} can be calculated as:

$$P_{muscle} = \vec{F}_{muscle} \cdot \vec{V}_{insertion} - \vec{F}_{muscle} \cdot \vec{V}_{origin} \quad (1)$$

where $\vec{F}_{muscle}$ is the muscle forces, $\vec{V}_{origin}$ and $\vec{V}_{insertion}$ are the velocities of the origin and insertion point, respectively [28]. The OpenSim model provided the coordinates of the origins and insertions in the local segment frames during walking. Using customized MATLAB codes, we transformed

the coordinates of the origins and insertions from the local segment frames to the global frame. The velocities were then calculated by central difference method. The mechanical energy produced by muscle W_{muscle} can be determined with the integration of muscle power P_{muscle} in selected periods from t_1 to t_2 as:

$$W_{muscle} = \int_{t_1}^{t_2} P_{muscle} \cdot dt \tag{2}$$

The mechanical work produced by the attachment points of muscles define the energy flow via individual muscles. The positive work presents the mechanical energy flow out from muscle, while the negative work shows the mechanical energy flow into muscle.

We selected 32 lower-extremity muscle groups in which to identify the energy flow and functional behaviors of individual muscles that included gluteus maximus (GMAX), gluteus medius (GMED), gluteus minimus (GMIN), Iliacus (ILI), psoas major (PSOAS), sartorius (SAR), adductor magnus (AMAG), rectus femoris (RF), long head of biceps femoris (BIFLH), short head of biceps femoris (BIFSH), semitendinosus (SEMITEN), semimembranosus (SEMIMEM), vastus medialis (VASMED), vastus intermedius (VASINT), vastus lateralis (VASLAT), gastrocnemius medialis (GASMED), gastrocnemius lateralis (GASLAT), soleus (SOL), posterior tibialis (TP), peroneus longus (PEROLON), peroneus breves (PEROBRE), flexor digitorum (FLEXDIG), flexor hallucis (FLEXHAL), and anterior tibialis (TA). GMAX, GMED, GMIN, and AMAG were separated to three parts due to their relatively large fiber width. VASMED, VASINT, and VASLAT can be grouped as vastus muscles (VAS). GASMED and GASLAT can be grouped as gastrocnemius muscles (GAS).

C. Calculation of Muscle Function Indices

As described by Lai et al. [6], muscle-specific indices were used to characterize the muscle functional behaviors as strut-, spring-, motor-, and damper-like based on mechanical work produced by individual muscles. Stance phase is divided into four sub-phases: collision, rebound, preload and push-off [16]. In this study, function indices analysis is conducted based on the mechanical work produced by individual muscles during different walking phases.

The strut index i_{struct} describes the proportion of muscle-tendon unit force contributes to muscle work. Therefore, the strut index could be calculated with the ration of muscle work over the normalized muscle force impulse:

$$i_{struct} = \max\left[\frac{(t_2 - t - 1)\int_{t_1}^{t_2} |P_c^m| dt}{\boldsymbol{l}_{cha}\int_{t_1}^{t_2} |F_c^m| dt}, 0\right] \times 100\% \tag{3}$$

where P_c^m and F_c^m are the power and force generated by muscle; l_{cha} is a characteristic length factor. According to McMahon and Cheng [29], muscle-tendon units functionally behave as springs during running. Therefore, the characteristic length factor can be determined to maximize the spring index with data from running trials. The spring index i_{spring} describes the functional behaviors as absorbing energy during compression and returning energy during generation.

$$i_{spring} = \frac{2.\min\left(\left|W_c^-\right|, \left|W_g^+\right|\right)}{\left|W_{Total}^-\right| + \left|W_{Total}^+\right|} \tag{4}$$

where W_c^- is negative work released during compression phase; W_g^+ is positive work produced during generation phase; W_{total}^- is total negative work; W_{total}^+ is total positive work. Compression and generation phases are defined based on the length of muscle slack length. Motor index i_{motor} can be calculated to characterize work generation for each muscle as:

$$i_{motor} = \frac{\left|W_{Total}^+\right| - \min(\left|W_c^-\right|, \left|W_g^+\right|)}{\left|W_{Total}^-\right| + \left|W_{Total}^+\right|} \times (100\% - i_{struct}) \tag{5}$$

Damper index i_{damper} can be determined to characterize mechanical work dissipation for each muscle as:

$$i_{damper} = \frac{\left|W_{Total}^-\right| - \min(\left|W_c^-\right|, \left|W_g^+\right|)}{\left|W_{Total}^-\right| + \left|W_{Total}^+\right|} \times (100\% - i_{struct}) \tag{6}$$

D. Statistical Analysis

The statistical analysis was performed to evaluate whether mechanical muscle work and functional behaviors change with different speeds from slow to fast walk using SPSS 20.0 software (IBM, USA). For each condition, means and standard deviations of muscle work as well as function indices in four different sub-phases were calculated across all subjects and trials. They were then analyzed separately by using the analysis of variance (ANOVA) with repeated measurements based on a linear mixed model approach considering intra- and inter-subject variability (random effects: subjects and trials; fixed effects: walking speed; significance level $p = 0.05$). For *post-hoc* processing, we used Fisher's least significant difference (LSD) multiple comparison based on the least-squared means to compare speed conditions with each other in order to investigate which walking speed exacted a significant change in muscle work and functional behaviors.

III. Results

The mechanical energy flow via individual muscles during four sub-phases at normal walking speed was presented in Figure 1. During collision, SOL along with TA and TP transferred mechanical energy from shank to foot, while GMAX, GASMED, and GASLAT released energy to both attached segments. The hip flexor muscles (ILI and PSOAS) and knee extensor muscles (VAS and RF) absorbed energy from both attached segments. During rebound, TP imported energy to shank and foot. Besides, BIFLH transported energy from shank to pelvis during collision and rebound. During preload, RF started to transfer energy from shank to pelvis and GMAX transferred energy from thigh to pelvis. Also, TA released energy to shank and foot. During push-off, TA transferred

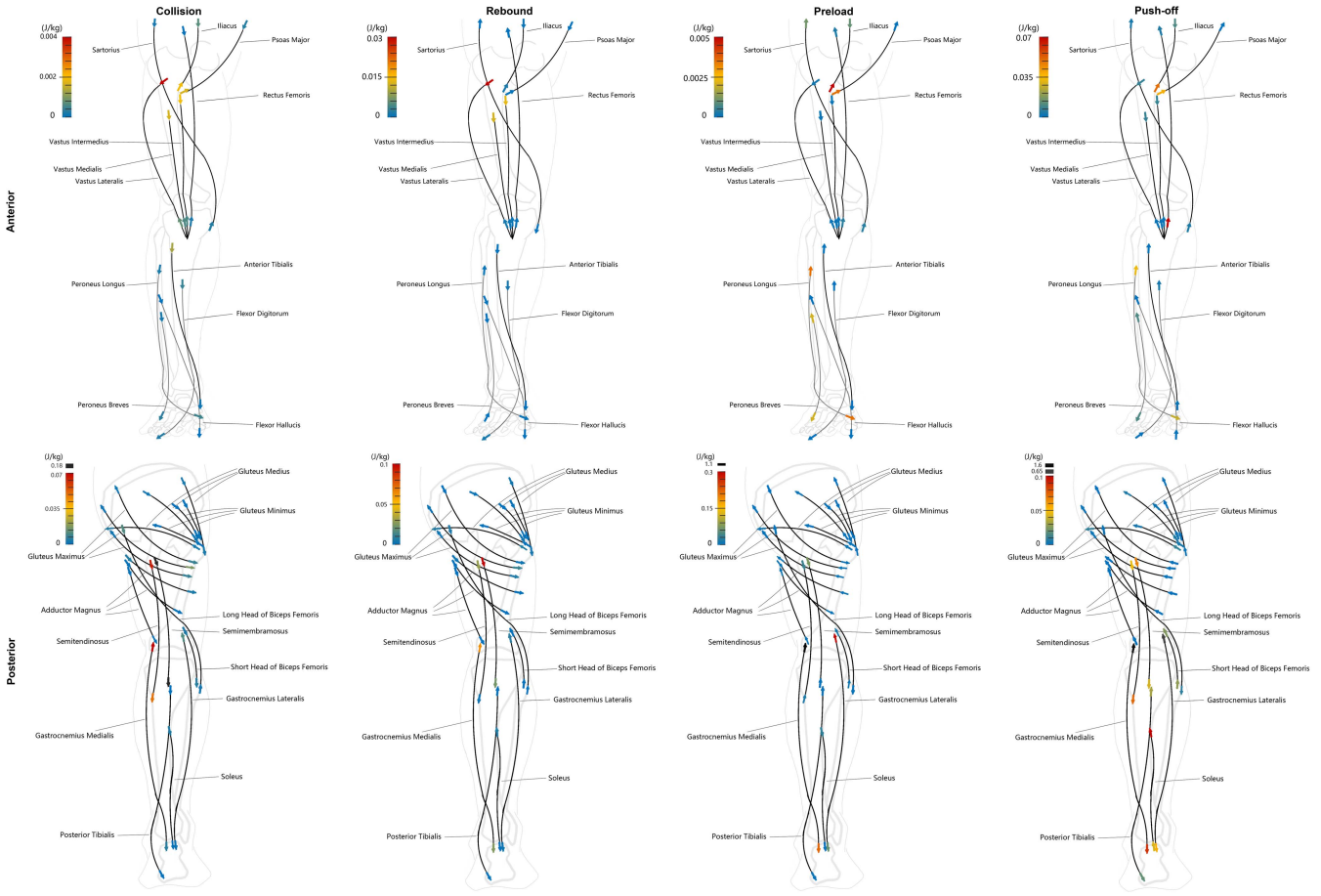

Fig. 1. Mechanical energy flow via individual muscles during four sub-phases at normal speed. Arrows depict the mechanical work produced by muscles and the direction of mechanical energy flow. Out from muscle, positive work; into muscle, negative work.

energy from foot to shank, while the ankle plantar flexor muscles (GAS, SOL, and TP) generated and released a great amount of mechanical work to both attached segments.

The muscle function indices at normal walking were used to demonstrate the change of muscle behaviors during four different sub-phases (Figure 2) and the whole stance phase (Supplementary Figure 1), while the variation trends under slow and fast speed were similar (Figure 3). GMAX showed motor-like function during the whole stance phase, and the motor index dominated during collision (almost 100%). GMED and GMIN acted as motor during collision, preload and push-off, but as strut during rebound. AMAG mainly functioned as damper during the first half of the stance phase, and as strut during the second half. ILI and PSOAS behaved as damper during all the four sub-phases in which the damper indices reached the peak during push-off (more than 95%). SEMITEN and SEMIMEM acted as damper during rebound, but as motor during other three sub-phases in which the motor index increased to the maximum during preload. VAS showed dominant damper-like function (more than 80%) during all the stance phase except preload (around 50%). BIFSH mostly showed motor-like function during all the sub-phases except rebound (as equally strut and motor). BIFLH mainly acted as damper during the first half of the stance phase, and as motor during the second half. RF behaved like damper during all the sub-phases except preload (as strut). PEROBRE and PEROLON functioned as strut in the first three sub-phases, but as motor during push-off. TP functioned as strut during the first half of the stance phase, but as motor during the second half. GAS and SOL mainly acted as motor during collision, preload and push-off, but as strut during rebound. In addition, it should be noticed that the functions of TA as well as FLEXDIG and FLEXHAL behaved quite differently during varied sub-phases from damper (collision) to strut (rebound), equally strut-motor (preload) and then to principal motor (push-off).

Figure 4 depicts the relevance of the function indices to walking speeds of 12 major muscles at different sub-phases. These muscles were selected from all 32 muscles based on the relatively large variations at different speeds. Details on the function indices of each muscle under different speeds during collision, rebound, preload, and push-off can be found in Supplementary Table I. During collision, with walking speed increasing, the strut indices of GMED2 and hip flexor muscles (ILI and PSOAS) decreased. The muscles surrounding knee (SAR, SEMITEN, VAS) showed more behavior as damper rather than strut. The motor indices of muscles surrounding ankle (SOL, PEROLON, GASMED) increased. During rebound, the motor indices of muscles surrounding

TABLE I

MECHANICAL ENERGY FLOW OF MAJOR MUSCLES ACTED ON PROXIMAL SEGMENTS AT DIFFERENT WALKING SPEEDS

Muscle	Speed	Segment	Collision	Rebound	Preload	Push-off
GMAX	Fast	Pelvis	8.398±2.361[a]	7.682±2.537[a]	6.180±0.693[a]	6.912±0.777[a]
	Normal	Pelvis	4.903±2.375[b]	4.846±2.562[b]	3.135±0.742[b]	2.705±0.835[b]
	Slow	Pelvis	6.660±2.376[a,b]	6.844±2.563[a,b]	4.255±0.74[a,b]	4.032±0.838[a,b]
GMED	Fast	Pelvis	-0.587±1.346[a]	0.656±2.425[a]	11.212±1.640[a]	23.239±2.624[a]
	Normal	Pelvis	0.035±1.391[a,b]	3.179±2.508[a,b]	9.429±1.645[a,b]	12.296±2.964[a,b]
	Slow	Pelvis	3.002±1.389[b]	5.233±2.505[b]	10.952±1.646[b]	11.924±2.965[b]
GMIN	Fast	Pelvis	-0.943±0.157[a]	-2.301±0.390[a]	3.345±0.538[a]	11.546±1.075[a]
	Normal	Pelvis	-1.340±0.177[a,b]	-0.472±0.432[a,b]	3.305±0.595[a]	6.244±1.189[b]
	Slow	Pelvis	-0.745±0.176[b]	0.241±0.430[b]	3.567±0.593[a]	5.539±1.183[b]
AMAG	Fast	Pelvis	-7.420±0.968[a]	-5.220±0.505[a]	0.098±0.019[a]	1.001±0.171[a]
	Normal	Pelvis	-6.567±1.045[a,b]	-2.100±0.575[a,b]	0.015±0.023[a]	0.492±0.201[a,b]
	Slow	Pelvis	-5.252±1.042[b]	-2.133±0.571[b]	0.010±0.023[a]	0.313±0.202[b]
ILI	Fast	Pelvis	-0.581±0.383[a]	-0.052±0.218[a]	-0.759±0.474[a]	-11.400±5.853[a]
	Normal	Pelvis	-0.667±0.407[a]	-0.424±0.263[a]	-0.913±0.513[a]	-10.847±6.378[a]
	Slow	Pelvis	-0.305±0.408[a]	-0.321±0.259[a]	-0.141±0.517[a]	-6.578±6.419[a]
PSOAS	Fast	Pelvis	-0.149±0.285[a]	-0.003±0.012[a]	0.006±0.043[a]	1.592±5.581[a]
	Normal	Pelvis	-0.261±0.296[a]	-0.043±0.016[a]	0.019±0.054[a]	0.060±5.718[a]
	Slow	Pelvis	-0.001±0.296[a]	-0.016±0.015[a]	0.106±0.052[a]	1.848±5.714[a]
SAR	Fast	Pelvis	-0.140±0.050[a]	0.015±0.010[a]	0.782±0.445[a]	4.958±1.549[a]
	Normal	Pelvis	-0.140±0.060[a]	0.007±0.012[a]	1.053±0.519[a]	2.864±1.703[a]
	Slow	Pelvis	-0.106±0.060[a]	0.003±0.012[a]	0.956±0.515[a]	2.832±1.694[a]
RF	Fast	Pelvis	-1.791±0.901[a]	-11.908±6.252[a]	0.645±0.317[a]	16.071±7.405[a]
	Normal	Pelvis	-0.016±1.099[a]	0.101±7.964[a]	0.264±0.411[a]	4.477±9.411[a]
	Slow	Pelvis	-0.390±1.078[a]	2.865±7.717[a]	0.221±0.395[a]	3.969±9.128[a]
VASMED	Fast	Thigh	-1.691±0.774[a]	-12.873±5.947[a]	-0.015±0.046[a]	-0.299±2.825[a]
	Normal	Thigh	-1.607±0.899[a]	-12.718±6.860[a,b]	-0.101±0.056[a]	-7.294±3.662[a]
	Slow	Thigh	-0.285±0.890[a]	-3.569±6.799[b]	-0.070±0.055[a]	-0.367±3.523[a]
VASINT	Fast	Thigh	-1.950±0.880[a]	-13.682±6.276[a]	-0.016±0.032[a]	-0.252±2.929[a]
	Normal	Thigh	-1.862±1.015[a]	-13.707±7.245[a]	-0.067±0.039[a]	-7.553±3.794[a]
	Slow	Thigh	-0.316±1.006[a]	-3.540±7.179[b]	-0.044±0.038[a]	-0.377±3.651[a]
VASLAT	Fast	Thigh	-3.758±1.798[a]	-29.806±13.878[a]	-0.019±0.085[a]	-0.566±4.741[a]
	Normal	Thigh	-3.859±2.060[a]	-30.474±16.009[a]	-0.187±0.103[a]	-12.247±6.148[a]
	Slow	Thigh	-0.610±2.043[a]	-7.936±15.865[b]	-0.138±0.102[a]	-0.606±5.913[a]
SEMIMEM	Fast	Pelvis	-428.394±97.870[a]	-230.537±63.879[a]	96.734±36.294[a]	239.723±68.859[a]
	Normal	Pelvis	-181.994±109.858[b]	-101.828±71.711[b]	61.518±40.783[a]	62.099±77.552[b]
	Slow	Pelvis	-152.481±109.000[b]	-126.771±71.245[a,b]	67.164±40.605[a]	94.141±76.908[b]
SEMITEN	Fast	Pelvis	-98.523±24.615[a]	-87.666±32.845[a]	43.054±15.554[a]	145.336±30.772[a]
	Normal	Pelvis	-64.408±27.998[a]	-30.094±35.729[b]	29.923±18.730[a]	43.968±37.016[b]
	Slow	Pelvis	-56.117±27.750[a]	-49.103±35.607[a,b]	17.095±18.448[a]	18.673±36.467[b]
BIFLH	Fast	Pelvis	-19.665±4.428[a]	-13.340±3.317[a]	4.492±1.726[a]	13.185±2.550[a]
	Normal	Pelvis	-11.078±5.050[b]	-5.805±3.813[b]	3.363±2.026[a]	2.079±3.099[b]
	Slow	Pelvis	-8.801±5.003[b]	-6.338±3.785[b]	2.481±2.002[a]	0.760±3.040[b]
BIFSH	Fast	Thigh	-5.507±1.433[a]	0.145±0.080[a]	8.502±2.272[a]	42.752±11.399[a]
	Normal	Thigh	-3.986±1.628[a,b]	0.104±0.108[a]	6.880±2.980[a]	23.702±12.912[a,b]
	Slow	Thigh	-2.606±1.616[b]	0.019±0.101[a]	3.166±2.849[a]	21.467±12.796[b]
GASMED	Fast	Thigh	120.501±39.179[a]	94.345±31.676[a]	1363.204±244.612[a]	2587.058±372.509[a]
	Normal	Thigh	69.619±44.391[a]	64.388±37.287[a]	1088.744±261.534[a]	1658.474±424.394[b]
	Slow	Thigh	65.103±43.993[a]	64.094±36.887[a]	1329.574±269.605[a]	2288.774±425.989[a,b]
GASLAT	Fast	Thigh	21.367±6.182[a]	11.610±3.601[a]	309.891±65.934[a]	998.548±155.809[a]
	Normal	Thigh	11.190±7.137[a,b]	8.336±4.416[a]	251.351±74.923[a]	658.374±175.058[b]
	Slow	Thigh	6.895±7.053[b]	5.319±4.331[a]	297.134±78.225[a]	891.403±176.121[a,b]
SOL	Fast	Shank	0.711±1.868[a]	6.971±3.112[a]	20.079±9.428[a]	163.819±43.345[a]
	Normal	Shank	4.606±2.029[b]	6.897±3.431[a]	23.367±10.646[a]	93.541±48.941[a,b]
	Slow	Shank	2.593±2.026[a,b]	6.401±3.422[a]	17.207±10.757[a]	86.485±48.513[b]
TP	Fast	Shank	-0.069±0.040[a]	0.018±0.064[a]	1.956±1.699[a]	64.713±14.848[a]
	Normal	Shank	-0.031±0.044[a]	0.089±0.084[a]	3.979±2.217[a]	30.543±17.164[b]
	Slow	Shank	-0.095±0.045[a]	0.113±0.080[a]	0.454±2.194[a]	19.305±16.959[b]
TA	Fast	Shank	-2.392±0.929[a]	-0.073±0.031[a]	0.009±0.004[a]	0.578±0.357[a]
	Normal	Shank	-1.244±1.038[a,b]	-0.008±0.041[a]	0.001±0.006[a]	0.884±0.407[a]
	Slow	Shank	-0.482±1.030[b]	-0.006±0.039[a]	0.007±0.006[a]	0.268±0.411[a]
PEROLON	Fast	Shank	-1.649±0.585[a]	0.595±0.313[a]	2.906±1.883[a]	47.288±12.111[a]
	Normal	Shank	-0.192±0.643[b]	0.522±0.356[a]	3.273±2.544[a]	32.992±13.963[a]
	Slow	Shank	-0.370±0.640[b]	0.766±0.354[a]	0.940±2.382[a]	25.687±13.802[a]
PEROBRE	Fast	Shank	-0.451±0.074[a]	-0.052±0.027[a]	0.690±0.515[a]	13.823±3.513[a]
	Normal	Shank	-0.156±0.094[b]	-0.049±0.037[a]	0.647±0.700[a]	10.688±4.119[a]
	Slow	Shank	-0.137±0.091[b]	-0.003±0.034[a]	0.015±0.652[a]	6.921±4.071[a]
FLEXHAL	Fast	Shank	-0.016±0.004[a]	-0.001±0.002[a]	0.000±0.001[a]	0.415±0.305[a]
	Normal	Shank	-0.006±0.005[a]	-0.001±0.002[a]	0.000±0.001[a]	0.355±0.327[a]
	Slow	Shank	-0.012±0.005[a]	-0.001±0.002[a]	0.001±0.001[a]	0.337±0.320[a]
FLEXDIG	Fast	Shank	-0.722±0.144[a]	-0.038±0.020[a]	0.009±0.003[a]	0.702±1.052[a]
	Normal	Shank	-0.410±0.184[a]	-0.006±0.023[a]	0.003±0.004[a]	2.892±1.359[a]
	Slow	Shank	-0.336±0.177[a]	-0.014±0.023[a]	0.006±0.004[a]	0.375±1.309[a]

Data are mean±s.d. for all the trials across all the subjects. Different letters mean that the variable in a column differs significantly with each other ($p < 0.05$).

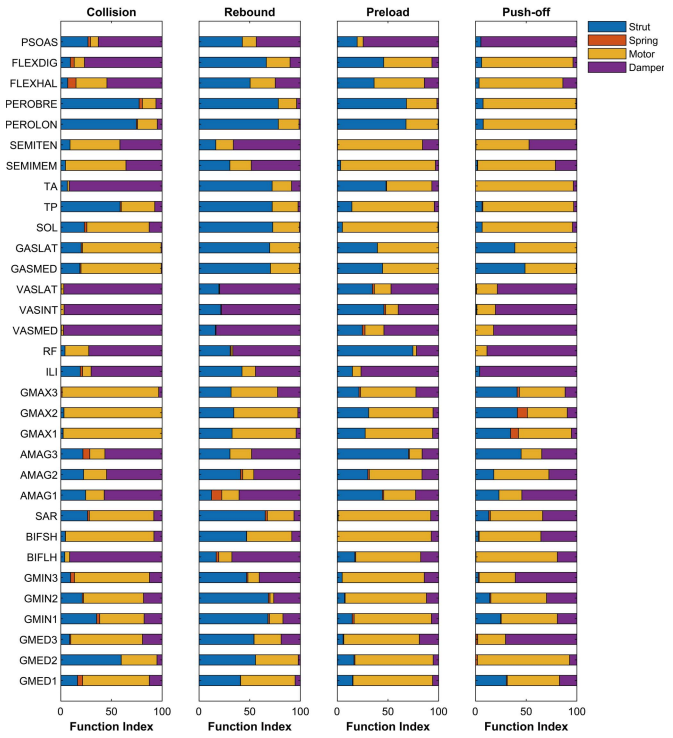

Fig. 2. Function indices of individual muscles during four sub-phases at normal speed. Calculated from mechanical work produced by individual muscles, function indices were used to characterize muscle functional behaviors as strut, spring, motor, and damper.

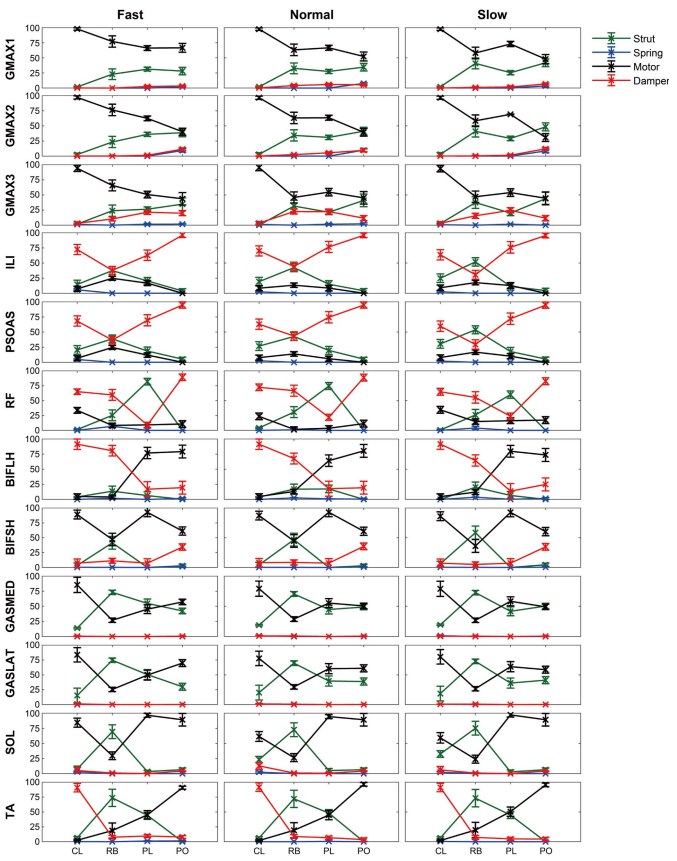

Fig. 3. Function indices of individual muscles during four sub-phases at different speeds. Means and standard deviations were depicted.

hip (GMIN, GMAX, ILI, PSOAS, SAR) grew with increasing walking speed. The damper indices of muscles surrounding knee (SEMITEN, SEMIMEM, BIFSH, VASINT) increased. The muscles surrounding ankle (SOL and TP) showed more motor behavior rather than strut. During preload, there were no significant change in the functional behaviors with increased walking speed, except slight enlarged strut-like function of RF and GAS. During push-off, the muscles surrounding hip acted as more motor rather than strut when the walking speed was raised. Meanwhile, the motor-like function of both GASMED and GASLAT increased.

IV. Discussions

A. Hip Flexor Muscles are the Main Contributors to Buffering Stride and Extensor Muscles are the Main Motors, While Adductor Muscles Mainly Transfer Energy to the Distal Segments During Collision and Rebound

GMAX acted as the motor to generate mechanical energy into pelvis and thigh during the whole stance phase, consistent with the study by Lai et al. [6]. The directions of the energy transfer in AMAG were different between early stance (collision, rebound) and late stance (preload, push-off). GMED and GMIN should not be regarded as a homogeneous region, because they are innervated segmented muscles with a separate innervation of each part, which define the hip adduction motion [30]. GMED1 transferred mechanical work from thigh to pelvis during collision and rebound, while GMED2 and GMED3 transferred energy from pelvis to thigh. But during preload and push-off, the energy flow direction of GMED2 and GMED3 was reversed to the same with GMED1. On the other hand, GMIN1 transported mechanical work from thigh to pelvis during the whole stance phase. GMIN2 and GMIN3 transferred energy from pelvis to thigh during the first three sub-phases, and changed its direction during push-off. Considering the magnitudes of the energy flow, the energy flow from thigh to pelvis was larger than the opposite direction during collision and rebound. Contrarily, this trend was reversed during preload and push-off, with more energy transmitted from pelvis to thigh. In a word, hip adductor muscles (GMED and GMIN) transfer energy to the distal segments during collision and rebound, but to the proximal segments during preload and push-off.

ILI behaved as damper to receive energy from pelvis and thigh to impede hip extension during the whole stance phase. PSOAS functioned as damper as well, but absorbed energy in the transferring process from thigh to pelvis during preload and push-off. The mechanical work absorbed was larger than transferred. SAR and RF are biarticular muscles across hip and knee. In previous studies [31], [32], [33], SAR was mainly regarded as hip flexor muscle and RF mainly contributed to knee extension. According to the functional behaviors, SAR acted as motor during collision, preload and push-off, but as strut during rebound. Meanwhile, RF acted as damper during collision, rebound and push-off, but as strut during preload. These were similar with the results from

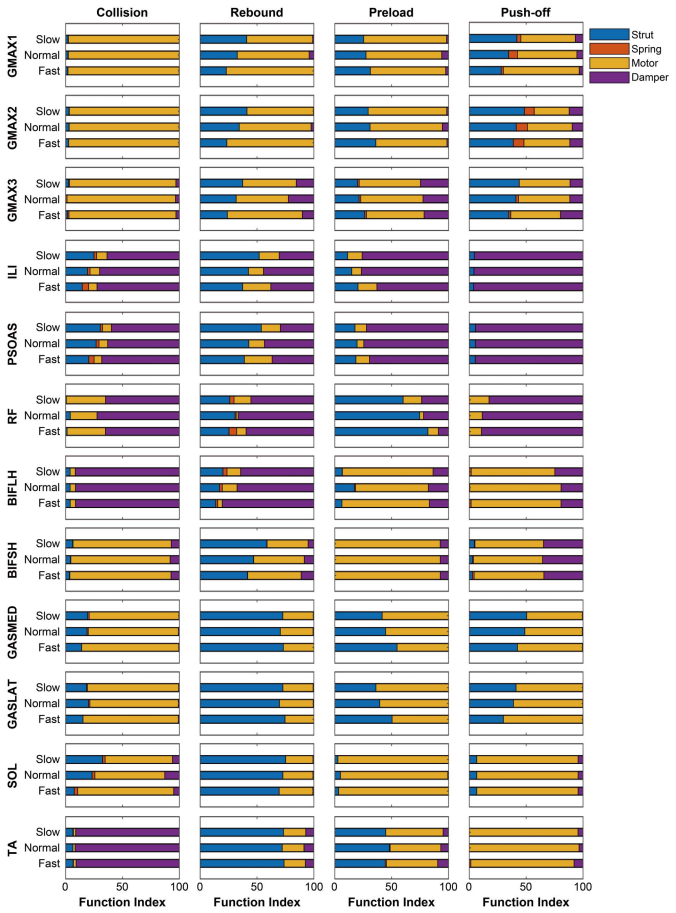

Fig. 4. Function indices of individual muscles at three speeds during different sub-phases. Calculated from mechanical work produced by individual muscles, function indices were used to characterize muscle functional behaviors as strut, spring, motor, and damper.

Neptune et al. [10], where the mechanical powers of the lower limb muscles showed the trends identical to those calculated in our study. RF absorbed energy from the early stance to the mid-stance, but accelerated the knee and hip into extension and redistributed the mechanical power to the pelvis in the late stance. In conclusion, hip flexor muscles absorbed energy for buffering stride and impeding extension motion from the beginning to the middle stance, and started to act as strut from preload to push-off.

B. Muscles Surrounding Knee Absorb Energy to Prepare for the Push-off During Preload

VAS kept absorbing energy from thigh and shank. The mechanical work during rebound was greater than the other three sub-phases. This was agreed with the previous research [34], in which the muscle activation patterns showed that the peaks of VASMED and VASLAT activation occurred during rebound. So, VAS contributed to knee extension mainly during rebound. BIFSH acted as strut during the whole stance phase. It transferred energy to the distal segments during collision but to the proximal segments from rebound to push-off. The transferred work during push-off was larger than the other three sub-phases. Both SEMITEN and SEMIMEM functioned as damper during rebound but as motor during the other three sub-phases by transferring energy from thigh to shank. They contributed the most during collision. This was supported by the results from Pandy and Andriacchi [35], where hamstrings (including SEMITEN and SEMIMEM) were significantly activated immediately after heel-strike and before foot flat. In another study, SEMIMEM was considered as spring during the whole gait cycle including stance and swing [6]. This may reveal that the energy absorbed by SEMITEN and SEMIMEM would be stored and returned during the swing phase. In previous studies [32], [36], [37], BIFLH was grouped with SEMITEN and SEMIMEM as hamstrings. But in this study, BIFLH behaved differently as spring during the first half of stance phase and as motor during the second half.

C. Ankle Dorsiflexor Flexor Muscles Contribute to Buffering the Stride While Ankle Plantar Flexor Muscles Provide Energy Generation for Propulsion

TA was the only ankle dorsiflexor muscle in this musculoskeletal model. Generally, TA was mainly active at the beginning of stance phase [32], [35], [38]. It acted as damper during collision to buffer the stride with transferring energy from shank to foot. TP and SOL were considered as motor during the whole stance phase except collision. They generated the most mechanical work during push-off. Pandy and Andriacchi [35] presented that SOL provided support and forward progression during the second half of stance phase. Apart from SOL, GAS were considered as another key contributors to ankle plantarflexion motion [3], [37]. However, Duysens et al. [39] showed that GASMED was more activated than GASLAT. Comparing the functional behaviors and energy flow via GASMED and GASLAT, this study demonstrated that GASMED generated more mechanical energy during the whole stance phase. In general, GAS acted as motor and the mechanical work was mainly produced during preload and push-off.

Meanwhile, FLE (flexor digitorum and flexor hallucis) provided body support during collision and rebound as they were strut-like and transferred energy to the distal segments. Since preload, FLE begun to produce positive work, and then transferred these energies to the proximal segments during push-off. As a result, FLE contributed to forward propulsion and body support during push-off. Comparing to previous studies [32], [35], [40], the peak contribution of PER (peroneus longus and peroneus breves) occurred during push-off with energy generation. The results also highlighted that PER could be regarded as spring during the whole stance phase. During collision and rebound, PER absorbed energy from shank and foot to buffer the stride. Observing from the ankle functional behaviors, PER were the principal factor to absorbing energy from ankle during collision. Therefore, the ankle plantar flexor muscles (TP, SOL, GASMED, FLE) except PER mainly provide plantarflexion motion during push-off. Ankle dorsiflexor muscle (TA) along with PER was the main contributor to buffering stride during collision. It is noteworthy that interpretation of muscle function involves not only the calculation of function indices but also the pattern of energy flow, because sometimes mechanical work changes does not corelate to functional behaviors. For instance, the peroneus

TABLE II
MECHANICAL ENERGY FLOW OF MAJOR MUSCLES ACTED ON DISTAL SEGMENTS AT DIFFERENT WALKING SPEEDS

Muscle	Speed	Segment	Collision	Rebound	Preload	Push-off
GMAX	Fast	Thigh	35.186±4.375[a]	45.162±3.890[a]	3.973±0.380[a]	0.163±0.235[a]
	Normal	Thigh	31.704±4.634[a,b]	20.258±4.317[b]	1.086±0.421[b]	0.563±0.278[b]
	Slow	Thigh	20.692±4.629[a]	18.174±4.292[b]	2.144±0.418[b]	0.085±0.280[a,b]
GMED	Fast	Thigh	2.926±1.379[a]	6.564±2.134[a]	-7.101±1.144[a]	-13.360±2.534[a]
	Normal	Thigh	2.252±1.430[a,b]	1.748±2.225[a,b]	-6.386±1.489[a,b]	-8.179±2.905[a,b]
	Slow	Thigh	-1.390±1.427[a]	-1.091±2.221[b]	-6.684±1.489[b]	-5.057±2.905[b]
GMIN	Fast	Thigh	0.991±0.166[a]	2.376±0.397[a]	-3.089±0.502[a]	-11.340±1.048[a]
	Normal	Thigh	1.400±0.187[a,b]	0.414±0.439[b]	-3.063±0.555[a]	-6.221±1.158[b]
	Slow	Thigh	0.770±0.185[b]	-0.362±0.438[b]	-3.307±0.553[a]	-5.147±1.153[b]
AMAG	Fast	Thigh	6.739±0.847[a]	1.921±0.171[a]	-0.069±0.008[a]	-0.931±0.166[a]
	Normal	Thigh	5.116±0.910[a,b]	0.552±0.199[a,b]	0.005±0.011[a,b]	-0.472±0.195[a,b]
	Slow	Thigh	4.305±0.907[b]	0.395±0.197[b]	-0.000±0.011[b]	-0.351±0.196[b]
ILI	Fast	Thigh	-2.234±1.089[a]	-0.166±0.697[a]	-2.737±1.627[a]	-58.185±15.274[a]
	Normal	Thigh	-1.840±1.163[a]	-1.493±0.847[a]	-4.654±2.027[a]	-51.239±18.029[a]
	Slow	Thigh	-1.113±1.170[a]	-0.858±0.833[a]	-0.819±1.984[a]	-32.871±17.890[a]
PSOAS	Fast	Shank	-1.899±1.135[a]	-0.012±0.061[a]	-2.201±1.416[a]	-48.922±12.647[a]
	Normal	Shank	-1.633±1.219[a]	-0.212±0.083[a]	-3.343±1.756[a]	-39.476±15.050[a]
	Slow	Shank	-0.910±1.216[a]	-0.050±0.077[a]	-0.879±1.717[a]	-26.481±14.859[a]
SAR	Fast	Shank	0.269±0.120[a]	0.012±0.005[a]	-0.205±0.207[a]	-4.760±1.213[a]
	Normal	Shank	0.268±0.134[a]	0.005±0.007[a]	-0.362±0.253[a]	-3.981±1.395[a,b]
	Slow	Shank	0.223±0.135[a]	0.005±0.007[a]	-0.065±0.255[a]	-2.188±1.384[b]
RF	Fast	Shank	-0.159±5.507[a]	-0.396±25.065[a]	-0.467±6.349[a]	-7.264±403.459[a]
	Normal	Shank	-0.198±7.569[a]	-0.550±35.198[a]	-0.370±8.936[a]	-71.318±527.553[a,b]
	Slow	Shank	-15.005±7.119[a]	-63.418±32.970[a]	-16.241±8.367[a]	-1196.711±500.806[b]
VASMED	Fast	Foot	-0.643±2.732[a]	-1.259±0.291[a]	-0.031±0.032[a]	-0.492±3.147[a]
	Normal	Foot	-0.594±3.851[a]	-0.672±0.337[b]	-0.067±0.045[a]	-1.035±4.419[a]
	Slow	Foot	-2.107±3.603[a]	-1.220±0.327[a,b]	-0.051±0.042[a]	-7.841±4.140[a]
VASINT	Fast	Foot	-0.741±3.436[a]	-1.464±0.340[a]	-0.031±0.031[a]	-0.528±3.779[a]
	Normal	Foot	-0.583±4.843[a]	-0.747±0.393[b]	-0.067±0.044[a]	-1.122±5.306[a]
	Slow	Foot	-2.671±4.532[a]	-1.384±0.382[a,b]	-0.046±0.041[a]	-9.412±4.970[a]
VASLAT	Fast	Foot	-1.342±5.194[a]	-2.637±0.586[a]	-0.046±0.035[a]	-0.838±6.938[a]
	Normal	Foot	-0.752±7.158[a]	-1.174±0.670[b]	-0.089±0.048[a]	-1.242±9.533[a]
	Slow	Foot	-4.135±6.853[a]	-2.328±0.657[a,b]	-0.031±0.046[a]	-17.428±9.132[a]
SEMIMEM	Fast	Foot	567.418±153.192[a]	76.781±21.463[a]	60.595±34.067[a]	-60.456±16.816[a]
	Normal	Foot	180.144±168.111[b]	22.929±23.926[b]	1.455±36.335[b]	-38.841±19.561[a]
	Slow	Foot	152.745±167.270[b]	31.180±23.784[b]	47.659±36.239[a,b]	-4.028±19.388[b]
SEMITEN	Fast	Thigh	108.449±29.956[a]	24.904±9.710[a]	20.765±14.884[a]	-68.941±21.555[a]
	Normal	Thigh	49.294±33.123[b]	2.557±10.464[b]	13.186±16.321[a]	-68.621±27.102[a]
	Slow	Thigh	52.090±32.927[b]	11.575±10.430[b]	12.990±16.245[a]	-4.950±26.386[b]
BIFLH	Fast	Thigh	-7.623±2.126[a]	-0.601±0.302[a]	1.164±0.906[a]	11.724±3.161[a]
	Normal	Thigh	-2.376±2.322[b]	-0.023±0.328[b]	2.389±1.094[a]	7.436±4.052[a,b]
	Slow	Thigh	-1.589±2.312[b]	-0.362±0.328[a,b]	0.439±1.077[a]	0.397±3.917[b]
BIFSH	Fast	Thigh	9.508±2.982[a]	0.275±0.086[a]	-2.637±1.844[a]	-36.766±9.188[a]
	Normal	Thigh	5.060±3.317[a,b]	-0.011±0.114[b]	-3.865±2.087[a]	-26.102±10.599[a,b]
	Slow	Thigh	2.918±3.295[b]	-0.013±0.108[b]	-1.22±2.105[a]	-18.187±10.482[b]
GASMED	Fast	Thigh	71.371±25.855[a]	-10.587±9.849[a]	303.381±60.725[a]	-36.478±101.755[a]
	Normal	Thigh	5.583±28.225[b]	-25.959±11.272[a]	183.532±63.202[b]	81.582±136.141[a]
	Slow	Thigh	16.081±28.098[b]	-18.434±11.379[a]	232.234±64.446[a,b]	209.333±130.861[a]
GASLAT	Fast	Thigh	14.768±4.463[a]	-1.417±1.239[a]	74.925±15.925[a]	5.708±30.018[a]
	Normal	Thigh	1.660±5.044[b]	-3.242±1.423[a]	50.541±16.989[a]	51.240±34.537[a]
	Slow	Thigh	2.635±5.006[b]	-1.668±1.437[a]	59.535±17.320[a]	64.123±34.486[a]
SOL	Fast	Shank	0.614±0.266[a]	1.592±1.073[a]	5.973±4.077[a]	-27.971±12.844[a]
	Normal	Shank	0.069±0.353[a]	0.420±1.396[a]	0.495±4.475[a]	-40.126±15.359[a]
	Slow	Shank	0.431±0.341[a]	1.322±1.341[a]	4.334±4.513[a]	-22.498±15.154[a]
TP	Fast	Shank	0.066±0.022[a]	0.018±0.100[a]	1.623±1.469[a]	48.655±12.234[a]
	Normal	Shank	0.037±0.025[a]	0.110±0.116[a]	3.867±1.981[a]	18.117±14.027[b]
	Slow	Shank	0.046±0.025[a]	0.051±0.117[a]	0.445±1.875[a]	19.721±13.867[b]
TA	Fast	Shank	0.569±0.210[a]	0.030±0.012[a]	0.033±0.014[a]	-0.665±0.501[a]
	Normal	Shank	0.077±0.232[b]	0.001±0.015[a]	0.006±0.017[a]	-0.851±0.533[a]
	Slow	Shank	0.233±0.230[b]	0.008±0.015[a]	0.005±0.017[a]	-0.447±0.536[a]
PEROLON	Fast	Foot	1.642±0.472[a]	0.448±0.273[a]	2.222±1.403[a]	40.206±10.531[a]
	Normal	Foot	0.464±0.533[b]	0.265±0.371[a]	3.318±1.847[a]	27.448±12.220[a]
	Slow	Foot	0.383±0.528[b]	0.096±0.345[a]	1.436±1.762[a]	23.792±12.062[a]
PEROBRE	Fast	Foot	0.726±0.124[a]	-0.063±0.071[a]	1.079±0.910[a]	14.067±3.989[a]
	Normal	Foot	0.338±0.159[b]	-0.083±0.081[b]	1.902±1.231[a]	5.188±4.675[a,b]
	Slow	Foot	0.196±0.153[b]	-0.159±0.080[b]	0.238±1.151[a]	9.469±4.604[b]
FLEXHAL	Fast	Foot	0.013±0.003[a]	-0.001±0.001[a]	0.000±0.001[a]	-0.408±0.317[a]
	Normal	Foot	0.002±0.004[b]	-0.000±0.001[a]	0.001±0.002[a]	-0.355±0.339[a]
	Slow	Foot	0.009±0.004[a,b]	-0.003±0.001[a]	0.002±0.002[a]	-0.340±0.332[a]
FLEXDIG	Fast	Foot	0.516±0.088[a]	0.027±0.019[a]	0.010±0.005[a]	-0.418±0.398[a]
	Normal	Foot	0.246±0.119[a,b]	0.013±0.021[b]	0.006±0.006[a]	-0.811±0.511[a]
	Slow	Foot	0.215±0.111[b]	0.037±0.021[b]	0.007±0.006[a]	-0.038±0.490[a]

Data are mean±s.d. for all the trials across all the subjects. Different letters mean that the variable in a column differs significantly with each other ($p < 0.05$).
Unit: $\times 10^{-3}$ J/kg.

longus shifted the energy flow from proximal segment during collision and rebound phase, but there was no apparent change in the function indices of the peroneus longus.

D. How Muscles and Energy Flow Affect Walking Speed?

The variations of energy performances with walking speeds of major muscles during each sub-phase were quantified (Table I and II). The results showed that during collision, 84.6% less energy was generated and inputted into shank via SOL from normal to fast walk, while TA absorbed 396.3% more energy from shank from slow to fast walk. Meanwhile, hip flexor muscles (ILI and PSOAS) and knee flexor muscle (BIFLH) received more energy. The increased energy induced from higher ground reaction forces during heel-strike were mainly restored by flexor muscles surrounding joints during collision. According to the joint-level energy analysis [4], hip and ankle absorbed more energy during collision with increased walking speed. Therefore, we assumed that these energies for stride buffering were mainly absorbed by the flexor muscles surrounding hip and ankle. However, BIFLH as the knee flexor muscle absorbed the most energy with an average of 16.898 $\times 10^{-3}$ J/kg increased in total from slow to fast walk. This might be caused by the different roles played by other muscles surrounding knee which are not included in this study.

During rebound, GMAX produced 148.5% more mechanical work under fast walking than slow walking and imported them to thigh, while GMED and AMAG transported more energy from pelvis to thigh. This suggested that more energy was transferred from pelvis to thigh via hip extensor and adductor muscles. During push-off, biceps femoris muscles including BIFSH and BIFLH inputted more energy to thigh (80.4%) and pelvis (534.2%), while plantar flexor muscles surrounding ankle (GAS and SOL) produced more mechanical work to thigh (54.8%) and shank (75.1%) from normal to fast walking. This indicated that the energy flow to the proximal segments had dramatically enhancement. In conclusion, knee flexor muscles and ankle plantar flexor muscles transferred more energy to the proximal segments for faster propulsion during push-off. These were in accordance with the results from our previous study [4], in which the ankle plantar flexor muscles were proven as the main contributors to generating more energy during push-off at faster walking speed.

E. Future Application

The above findings regarding the energy flow and functional behaviors of muscles would play important roles in the development of human-inspired assistive robotics (including humanoid robots, prostheses and exoskeletons). According to the previous researches [41], [42], [43], [44], [45], these robots are designed based on human motion (including walking, running, lifting, crouching and so on), which requires deep understanding of how the individual muscles work at different sub-phases. For example, with detecting the activities of muscles, human motion intention could be estimated, yielding more biological designs of exoskeleton and prosthesis. The sensing system could be set based on estimation of intended motion, which would improve the accuracy of switching between various tasks in daily lives. As the mechanical energy performances of muscles are analyzed, unpowered lower limb exoskeleton with muscle-assisting function could be developed based on the muscle energy flow of human walking. In the future, it might be possible to analyze the gait of patients with muscular deficits or to enable the construction of patient-specific rehabilitation robots. Also, this study could provide insights into designing the control systems of humanoid robots with artificial muscles. However, our models were built based on a standard OpenSim model in which the tendons of the muscles do not have compliance. In future, more biofidelic muscle models could be developed with compliance to produce more realistic results.

V. Conclusion

By calculating and statistically analyzing the speed-varying functional behaviors and mechanical work, this study provides the most comprehensive description available to date of energetic contributions of 32 major muscles in the human body at four different sub-phases during the stance of walking. The results demonstrate that, during collision, hip flexor (ILI and PSOAS) and ankle dorsiflexor (TA) muscles absorb energy to buffer the stride. The increased energy induced from heel-stride when walking faster is mainly absorbed by the flexor muscles surrounding hip and ankle. During rebound, muscles in the posterior side (GMAX, GAS, TP, SOL) generate energy, and more energy caused by the increasing walking speed is transferred from pelvis via hip extensor and adductor muscles. During preload, the mechanical work produced for preparation for push-off is absorbed by the muscles surrounding knee (VAS, SEMITEN, SEMIMEM). During push-off, the energy for forward propulsion is primarily generated by ankle plantar flexor muscles (GAS, SOL, TP, PER, FLE). Among them, GAS and SOL are the main contributors to transfer more energy to the proximal segments for propulsion at fast walking speed. These findings will assist in future steps toward better understanding of human musculoskeletal behaviors during locomotion and provide fundamental principles for the bio-inspired design of related assistive devices from motors performance enhancement to rehabilitation.

References

[1] D. Gordon, E. Robertson, and D. A. Winter, "Mechanical energy generation, absorption and transfer amongst segments during walking," *J. Biomech.*, vol. 13, no. 10, pp. 845–854, Jan. 1980, doi: 10.1016/0021-9290(80)90172-4.

[2] K. E. Zelik, K. Z. Takahashi, and G. S. Sawicki, "Six degree-of-freedom analysis of hip, knee, ankle and foot provides updated understanding of biomechanical work during human walking," *J. Experim. Biol.*, vol. 218, no. 6, pp. 876–886, Mar. 2015, doi: 10.1242/jeb.115451.

[3] A. G. Schache, N. A. T. Brown, and M. G. Pandy, "Modulation of work and power by the human lower-limb joints with increasing steady-state locomotion speed," *J. Experim. Biol.*, vol. 218, pp. 2472–2481, Jan. 2015, doi: 10.1242/jeb.119156.

[4] Z. Hu et al., "Speed-related energy flow and joint function change during human walking," *Frontiers Bioengineering Biotechnol.*, vol. 9, May 2021, Art. no. 666428, doi: 10.3389/fbioe.2021.666428.

[5] N. Peyrot et al., "Mechanical work and metabolic cost of walking after weight loss in obese adolescents," *Med. Sci. Sports Exercise*, vol. 42, no. 10, pp. 1914–1922, Oct. 2010, doi: 10.1249/MSS.0b013e3181da8d1e.

[6] A. K. M. Lai, A. A. Biewener, and J. M. Wakeling, "Muscle-specific indices to characterise the functional behaviour of human lower-limb muscles during locomotion," *J. Biomech.*, vol. 89, pp. 134–138, May 2019, doi: 10.1016/j.jbiomech.2019.04.027.

[7] M. H. Dickinson, C. T. Farley, R. J. Full, M. A. R. Koehl, R. Kram, and S. Lehman, "How animals move: An integrative view," *Science*, vol. 288, no. 5463, pp. 100–106, Apr. 2000, doi: 10.1126/science.288.5463.100.

[8] J.-P. Kulmala et al., "Walking and running require greater effort from the ankle than the knee extensor muscles," *Med. Sci. Sports Exerc.*, vol. 48, no. 11, pp. 2181–2189, Nov. 2016, doi: 10.1249/MSS.0000000000001020.

[9] M. Qiao and D. L. Jindrich, "Leg joint function during walking acceleration and deceleration," *J. Biomech.*, vol. 49, no. 1, pp. 66–72, Jan. 2016, doi: 10.1016/j.jbiomech.2015.11.022.

[10] R. R. Neptune, F. E. Zajac, and S. A. Kautz, "Muscle force redistributes segmental power for body progression during walking," *Gait Posture*, vol. 19, no. 2, pp. 194–205, Apr. 2004, doi: 10.1016/S0966-6362(03)00062-6.

[11] D. J. Farris and G. S. Sawicki, "Human medial gastrocnemius force–velocity behavior shifts with locomotion speed and gait," *Proc. Nat. Acad. Sci. USA*, vol. 109, no. 3, pp. 977–982, Jan. 2012, doi: 10.1073/pnas.1107972109.

[12] T. N. Giest and Y.-H. Chang, "Biomechanics of the human walk-to-run gait transition in persons with unilateral transtibial amputation," *J. Biomech.*, vol. 49, no. 9, pp. 1757–1764, Jun. 2016, doi: 10.1016/j.jbiomech.2016.04.004.

[13] A. Lai, G. A. Lichtwark, A. G. Schache, Y.-C. Lin, N. A. T. Brown, and M. G. Pandy, "In vivo behavior of the human soleus muscle with increasing walking and running speeds," *J. Appl. Physiol.*, vol. 118, no. 10, pp. 1266–1275, May 2015, doi: 10.1152/japplphysiol.00128.2015.

[14] A. A. Biewener and M. A. Daley, "Unsteady locomotion: Integrating muscle function with whole body dynamics and neuromuscular control," *J. Experim. Biol.*, vol. 210, no. 17, pp. 2949–2960, Sep. 2007, doi: 10.1242/jeb.005801.

[15] A. Lai, A. G. Schache, N. A. T. Brown, and M. G. Pandy, "Human ankle plantar flexor muscle–tendon mechanics and energetics during maximum acceleration sprinting," *J. Roy. Soc. Interface*, vol. 13, no. 121, Aug. 2016, Art. no. 20160391, doi: 10.1098/rsif.2016.0391.

[16] K. E. Zelik and A. D. Kuo, "Human walking isn't all hard work: Evidence of soft tissue contributions to energy dissipation and return," *J. Exp. Biol.*, vol. 213, no. 24, pp. 4257–4264, Dec. 2010, doi: 10.1242/jeb.044297.

[17] A. L. Hof, H. Elzinga, W. Grimmius, and J. P. K. Halbertsma, "Speed dependence of averaged EMG profiles in walking," *Gait Posture*, vol. 16, no. 1, pp. 78–86, Aug. 2002, doi: 10.1016/S0966-6362(01)00206-5.

[18] Y. P. Ivanenko, R. E. Poppele, and F. Lacquaniti, "Five basic muscle activation patterns account for muscle activity during human locomotion," *J. Physiol.*, vol. 556, no. 1, pp. 267–282, 2004, doi: 10.1113/jphysiol.2003.057174.

[19] L. Ren, R. K. Jones, and D. Howard, "Dynamic analysis of load carriage biomechanics during level walking," *J. Biomech.*, vol. 38, no. 4, pp. 853–863, Apr. 2005, doi: 10.1016/j.jbiomech.2004.04.030.

[20] C. Angeloni, A. Cappozzo, F. Catani, and A. Leardini, "Quantification of relative displacement of skin- and plate-mounted markers with respect to bones," *J. Biomech.*, vol. 26, no. 864, p. 60, 1993.

[21] E. H. Garling et al., "Soft-tissue artefact assessment during step-up using fluoroscopy and skin-mounted markers," *J. Biomech.*, vol. 40, pp. S18–S24, Jan. 2007, doi: 10.1016/j.jbiomech.2007.03.003.

[22] A. Cappozzo, F. Catani, U. D. Croce, and A. Leardini, "Position and orientation in space of bones during movement: Anatomical frame definition and determination," *Clin. Biomech.*, vol. 10, no. 4, pp. 171–178, 1995, doi: 10.1016/0268-0033(95)91394-T.

[23] A. Cappozzo, "Gait analysis methodology," *Hum. Mov. Sci.*, vol. 3, nos. 1–2, pp. 27–50, Mar. 1984, doi: 10.1016/0167-9457(84)90004-6.

[24] S. S. H. U. Gamage and J. Lasenby, "New least squares solutions for estimating the average centre of rotation and the axis of rotation," *J. Biomech.*, vol. 35, no. 1, pp. 87–93, Jan. 2002, doi: 10.1016/S0021-9290(01)00160-9.

[25] A. Seth et al., "OpenSim: Simulating musculoskeletal dynamics and neuromuscular control to study human and animal movement," *PLOS Comput. Biol.*, vol. 14, no. 7, Jul. 2018, Art. no. e1006223, doi: 10.1371/journal.pcbi.1006223.

[26] M. Millard, T. Uchida, A. Seth, and S. L. Delp, "Flexing computational muscle: Modeling and simulation of musculotendon dynamics," *J. Biomech. Eng.*, vol. 135, no. 2, Feb. 2013, Art. no. 021005, doi: 10.1115/1.4023390.

[27] D. G. Thelen and F. C. Anderson, "Using computed muscle control to generate forward dynamic simulations of human walking from experimental data," *J. Biomech.*, vol. 39, no. 6, pp. 1107–1115, Jan. 2006, doi: 10.1016/j.jbiomech.2005.02.010.

[28] F. E. Zajac, R. R. Neptune, and S. A. Kautz, "Biomechanics and muscle coordination of human walking," *Gait Posture*, vol. 16, no. 3, pp. 215–232, Dec. 2002, doi: 10.1016/S0966-6362(02)00068-1.

[29] T. A. McMahon and G. C. Cheng, "The mechanics of running: How does stiffness couple with speed?" *J. Biomech.*, vol. 23, no. 1, pp. 65–78, Feb. 1990, doi: 10.1016/0021-9290(90)90042-2.

[30] A. Al-Hayani, "The functional anatomy of hip abductors," *Folia Morpholog.*, vol. 68, no. 2, pp. 98–103, May 2009, [Online]. Available: http://www.ncbi.nlm.nih.gov/pubmed/19449297

[31] S. A. Kautz, M. L. Hull, and R. R. Neptune, "A comparison of muscular mechanical energy expenditure and internal work in cycling," *J. Biomech.*, vol. 27, no. 12, pp. 1459–1467, Dec. 1994, doi: 10.1016/0021-9290(94)90195-3.

[32] K. Sasaki and R. R. Neptune, "Individual muscle contributions to the axial knee joint contact force during normal walking," *J. Biomech.*, vol. 43, no. 14, pp. 2780–2784, Oct. 2010, doi: 10.1016/j.jbiomech.2010.06.011.

[33] P. A. Iturralde and G. Torres-Oviedo, "Corrective muscle activity reveals subject-specific sensorimotor recalibration," *Eneuro*, vol. 6, no. 2, Mar. 2019, Art. no. ENEURO.0358, doi: 10.1523/ENEURO.0358-18.2019.

[34] F. A. Panizzolo, S. Lee, T. Miyatake, D. M. Rossi, C. Siviy, J. Speeckaert, I. Galiana, and C. J. Walsh, "Lower limb biomechanical analysis during an unanticipated step on a bump reveals specific adaptations of walking on uneven terrains," *J. Exp. Biol.*, vol. 220, no. 22, pp. 4169–4176, 2017, doi: 10.1242/jeb.161158.

[35] M. G. Pandy and T. P. Andriacchi, "Muscle and joint function in human locomotion," *Annu. Rev. Biomed. Eng.*, vol. 12, pp. 401–433, Aug. 2010, doi: 10.1146/annurev-bioeng-070909-105259.

[36] K. Sasaki and R. R. Neptune, "Muscle mechanical work and elastic energy utilization during walking and running near the preferred gait transition speed," *Gait Posture*, vol. 23, no. 3, pp. 383–390, Apr. 2006, doi: 10.1016/j.gaitpost.2005.05.002.

[37] J. Markowitz and H. Herr, "Human leg model predicts muscle forces, states, and energetics during walking," *PLOS Comput. Biol.*, vol. 12, no. 5, May 2016, Art. no. e1004912, doi: 10.1371/journal.pcbi.1004912.

[38] A. S. Ghafari, A. Meghdari, and G. R. Vossoughi, "Biomechanical analysis for the study of muscle contributions to support load carrying," *Proc. Inst. Mech. Eng., C, J. Mech. Eng. Sci.*, vol. 224, no. 6, pp. 1287–1298, Jun. 2010, doi: 10.1243/09544062JMES1559.

[39] J. Duysens, B. M. H. van Wezel, T. Prokop, and W. Berger, "Medial gastrocnemius is more activated than lateral gastrocnemius in sural nerve induced reflexes during human gait," *Brain Res.*, vol. 727, nos. 1–2, pp. 230–232, Jul. 1996, doi: 10.1016/0006-8993(96)00525-2.

[40] F. Fraysse, R. Dumas, L. Cheze, and X. Wang, "Comparison of global and joint-to-joint methods for estimating the hip joint load and the muscle forces during walking," *J. Biomech.*, vol. 42, no. 14, pp. 2357–2362, Oct. 2009, doi: 10.1016/j.jbiomech.2009.06.056.

[41] B. Corteville, E. Aertbelien, H. Bruyninckx, J. D. Schutter, and H. Van Brussel, "Human-inspired robot assistant for fast point-to-point movements," in *Proc. IEEE Int. Conf. Robot. Autom.*, Apr. 2007, pp. 3639–3644, doi: 10.1109/ROBOT.2007.364036.

[42] J. M. Romano, K. Hsiao, G. Niemeyer, S. Chitta, and K. J. Kuchenbecker, "Human-inspired robotic grasp control with tactile sensing," *IEEE Trans. Robot.*, vol. 27, no. 6, pp. 1067–1079, Dec. 2011, doi: 10.1109/TRO.2011.2162271.

[43] X. Liu, Z. Zhou, J. Mai, and Q. Wang, "Real-time mode recognition based assistive torque control of bionic knee exoskeleton for sit-to-stand and stand-to-sit transitions," *Robot. Auto. Syst.*, vol. 119, pp. 209–220, Sep. 2019, doi: 10.1016/j.robot.2019.06.008.

[44] A. D. Ames, "Human-inspired control of bipedal walking robots," *IEEE Trans. Autom. Control*, vol. 59, no. 5, pp. 1115–1130, May 2014, doi: 10.1109/TAC.2014.2299342.

[45] M. K. Ishmael, D. Archangeli, and T. Lenzi, "Powered hip exoskeleton improves walking economy in individuals with above-knee amputation," *Nature Med.*, vol. 27, no. 10, pp. 1783–1788, Oct. 2021, doi: 10.1038/s41591-021-01515-2.